Molecularly Imprinted Polymer (MIP)-Based Electrochemical Sensor for Determination of Amyloid β-42 in Alzheimer's Disease

S. Ninket, S. Pakapongpan, N. Plongthongkum, P. Namchaiw, and R. P. Poo-arporn*

Abstract—**Alzheimer's disease is the most common type of dementia caused by degeneration of the brain that affects a person's ability to function independently. Amyloid beta 42 (Aβ-42) is used as a biomarker for Alzheimer's disease detection. Increasing the sensitivity of early stage detection of Alzheimer's disease is challenging. This study mainly focused on the development of signal amplification of Aβ-42 detection using Graphene (G) and Carbon Dot (CD) which were modified on Screen-Printed Carbon Electrode (SPCE) to form graphene-carbon dot/ SPCE. The successful of modified SPCE was investigated by Cyclic Voltammetry (CV). The Molecularly Imprinted Polymer (MIP) was used for specific detection of Aβ-42. The MIP-based Aβ-42 sensor was prepared by polymerization of *o*-phenylenediamine (oPD) monomer jointly with Aβ-42 template on the modified SPCE using the Differential Pulse Voltammetry (DPV) technique. The results showed the optimum conditions for the MIP fabrication; an electropolymerization cycle of 15 cycles and elution time of 8 minutes. The MIP-based Aβ-42 sensor exhibited the detection range of Aβ-42 from 1 to 30 pg/ml with the linear range from 0.5 to 20 pg/ml, the R^2 from the regression curve of 0.9732 and a Limit of Detection (LOD) of 0.104 ng/ml. The developed MIP-based Aβ-42 sensor was suitable for Aβ-42 detection with cost effectiveness, high sensitivity, and easy to use.**

Index Terms—**Amyloid beta, electrochemical sensor, Molecularly Imprinted Polymer (MIP)**

I. INTRODUCTION

Alzheimer's disease is the most common type of dementia caused by the destruction of nerve cells that affects thinking and learning of the patients. Deterioration of the brain function leads to memory loss [1]. The formation of Amyloid Beta (Aβ) plaque is the pathological hallmark of Alzheimer's disease. Aβ is formed by the process of Amyloid Precursor Protein (APP) transforming into two isoforms, including Aβ-40 and Aβ-42. Aβ-42 was reported as a major component of the amyloid plaques and it is more cytotoxic than Aβ-40. The aggregation and plaque deposition in the brain of Aβ-42 directly links to the pathogenesis of Alzheimer's disease [2, 3]. Brain imaging is the most common way to observe the anatomical brain structure and the presence of Aβ that can be used to diagnose Alzheimer's disease along with mental state examination. However, this method has limitations because it has a high cost and the patients would have a brain imaging test only if they exhibit significant symptoms. Alternatively, Aβ-42 serves as a crucial biomarker for identification of the presence and progression of the disease. In addition, the shift in Aβ-42 level could be detected before the disease symptoms could be detected. Aβ-42 could be detected in Cerebrospinal Fluid (CSF) at high sensitivity. However, detection of Aβ-42 in the CSF has a very high risk as it requires lumbar puncture, so it is not widely used in clinical [4]. Aβ-42 can also be found in the blood. Even though, the sensitivity in the blood is not as high as in the CSF, detection of this protein in the blood is simple, highly accurate, rapid, and safe to the patients [5, 6].

The Electrochemical Sensor (ECS) is a technique developed and widely used in clinical practice because of their high sensitivity, rapid response and compatibility with miniaturization. The strengths of ECS are high detection efficiency and high target molecule stability. Therefore, it is the prerequisites for the creation of all sorts of sensors [7, 8]. The Molecularly Imprinted Polymer (MIP) is combined with electrochemical sensors and it has been of great interest in the quantitative detection of macromolecule and molecular complexes as well as biomarkers. MIP provides many advantages; it is the synthetic polymer which is specific to the target molecule, an imprinted site is comparable to the specificity of antibodies, the MIP has a high breakdown rate, it has high specificity and sensitivity, it responds quickly with easy preparation and low cost [8]. M. You et al. presented a MIP/aptamer-based electrochemical sensor as sandwich assay for Amyloid-β Oligomer (AβO) determining. The MIP/aptamer-based sensor showed a linear range of amyloid-β oligomer detection of 5 pg/ml to 10 ng/ml with a Limit of Detection (LOD) of 1.22 pg/ml [9]. Their results showed the linear range and LOD efficiency of MIP-based sensor.

Nanomaterials, such as gold nanoparticles, carbon nanotubes, and graphene, with the advantages of excellent conductivity, electrocatalytic activity and high surface area properties were used to improve the surface of the electrode by amplifying the signal of the sensor. Moreover, the Carbon Dot (CD) is a carbon-based nanomaterial whose size is below 10 nm. It is generally applied in electrochemical sensor for enhancement of conductivity, surface area and diverse electrochemical activities. García-Mendiola et al. presented an electrochemical DNA biosensor based on Carbon Nanodots (CDs) modified screen-printed gold electrode. They showed that that carbon dot cause an increment of the relative surface area and they can be involved in the oxidation and reduction processes [10].

Herein, this work mainly focused on the MIP-based electrochemical sensor for Aβ-42 detection using graphene-carbon dot for the signal amplification and MIP-based approach for selectivity of Aβ-42 detection. Additionally, the performances of the sensor were investigated to provide the optimal conditions i.e., electropolymerization, elution time,

and linear range of detection. This sensor can reduce the testing cost and increase the sensitivity of Alzheimer's disease detection.

II. MATERIAL AND METHOD

A. Graphene-Carbon Dot Modified SPCE Fabrication

Briefly, the carbon dot was synthesized by mixing Citric Acid (CA), urea and Dimethylformamide (DMF) then the solution was heated at 200 °C to form carbon dot. After synthesis, carbon dot was purified by ethyl acetate and petroleum ether [11].

The graphene-carbon dot composite was synthesized by mixing graphene and carbon dot under ultrasonication. After that, the working surface was modified by 10 µl of graphene-carbon dot composite and then allowed to dry in an incubator at 65 °C for 1 h.

B. The fabrication of MIP modified electrode

To fabricate the MIP, the oPD was deposited and electropolymerized on the graphene-carbon dot/SPCE to provide the imprint site between monomers and the Aβ-42. The oPD (50 mM) and Aβ-42 (0.05 mg/mL) pH 7 in PBS were mixed and dropped on graphene-carbon dot/SPCE before electropolymerization by CV technique for 15 cycles in the potential range from 0 to 1 V. Finally, Aβ-42 template was eluted by NaOH (5 mM) solution and wash with DI for 3 mins

Non-molecularly Imprinted Polymer (NIP) was prepared by the same condition without Aβ-42 template for providing the imprint site.

C. Electrochemical Measurement

The Autolab PGSTAT128N Metrohm and NOVA 2.1 software was used for all electrochemical measurements. All experiments were operated in 1 mM $K_3[Fe(CN)_6]/K_4[Fe(CN)_6]$ containing 0.1 M KCl.

The electrode modification steps were performed by CV technique in the potential range from −0.4 to 0.8 V, scan rate of 0.1 mV/s. For Aβ-42 detection step, Aβ-42 was incubated on MIP for 5 minutes then washed with DI for 1 minutes to remove nonspecific protein before investigated by DPV technique between –0.2 V and 0.4 V with a pulse amplitude of 0.05 V.

D. MIP-Based Aβ-42 Sensor Optimization

The optimization of MIP-based Aβ-42 sensor was studied based on cycle number of electropolymerization, elution time, and calibration curve. Firstly, the cycle number of electropolymerization was optimized by applying the CV cycle of 10, 15, 20 and 30 cycles to obtain the suitable thickness of monomer. Secondly, after performing the MIP-based Aβ-42 sensor, the Aβ-42 template was eluted in NaOH solution (5 mM) using different incubation times for 3, 5, 8, and 10 minutes. The optimal condition was the one that provided the slope of the calibration curve.

To generate a calibration curve, Aβ-42 protein was incubated at different concentrations from 0.5, 1, 5, 10, 20, and 30 pg/ml for 5 minutes and the DPV responses of each concentration were measured. The change of anodic peak current (ΔI) from DPV responses represented the rebinding performance which was calculated by Eq. (1).

$$\Delta I = I_{\text{before rebinding}} - I_{\text{after rebinding}} \tag{1}$$

E. Structural and Morphological Characterization

The Scanning Electron Microscope (SEM) and Energy Dispersive X-ray Spectroscopy (EDS) were used for morphology and element quantification, respectively for bare SPCE and graphene-carbon dot/SPCE.

III. RESULTS AND DISCUSSION

A. The Surface Morphology of Electrode modification

The surface morphology of bare SPCE and graphene-carbon dot /SPCE was observed using by SEM technique. The result was showed in Fig. 1. The SEM image showed the graphene-carbon aggregates on the bare SPCE surface. The approximated size of the graphene-carbon dot was 4.05 µm (Fig. 1A–B). However, the SEM technique could not be used to detect the carbon dot because the size of carbon dot deposited on graphene was smaller than 3 nm [11]. The Energy Dispersive Spectrometer (EDS) spectra also showed the coexistence of C, N, and O signals on the electrode. These results demonstrated the distribution of C 100 %wt on the G/SPCE (Fig. 1C) while the graphene-carbon dot/SPCE had the distribution of C 79.03 %wt, N 13.55 %wt, and O 7.41 %wt (Fig. 1D). These results indicated that carbon dot has been successful attach to graphene as the carbon dot surface contains N and O which were the components of the functional groups (C=O, C-O, C-O-C, O-H, N-H, C-N, C-N-C).
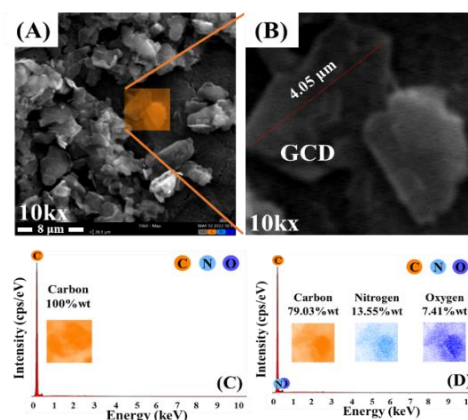

Fig. 1. The SEM images of graphene-carbon dot /SPCE (A), (B). The EDS analysis of G/SPCE (C) and graphene-carbon dot /SPCE (D).
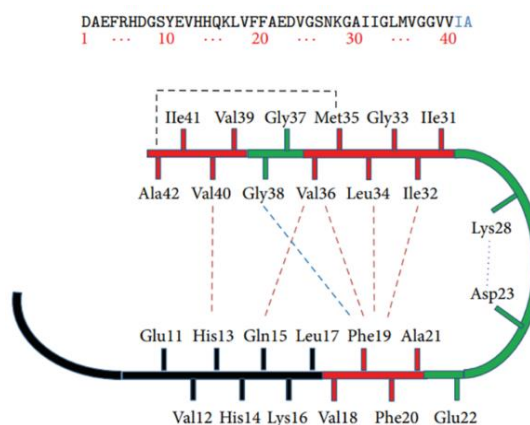

Fig. 2. The amino acid sequence of Aβ-42 [12].

B. Modified Electrode Electrochemical Characterization

CV technique was used to characterize the electrochemical property of the bare SPCE, graphene/SPCE and graphene-carbon dot/SPCE. The current response of 1 mM $K_3[Fe(CN)_6]/K_4[Fe(CN)_6]$ at graphene-carbon dot/SPCE (curve c of Fig. 3A) was higher than the bare SPCE and graphene (curve a and b of Fig. 3A). Because graphene can enhance the conductivity and surface area of an electrode [13] similar to the carbon dot which is the carbon-based material containing the heteroatoms of nitrogen and oxygen in carbon dot nanoparticles [11]. Basically, the carbon dot is applied in electrical applications because it is a high conductivity material which can improve electron transfer [14]. Moreover, the oxidation and reduction peaks of graphene-carbon dot/SPCE exhibited a bit shift of potential. These results confirmed that the graphene-carbon dot was successfully modified on SPCE to enlarge the electron transfer process and provide more surface area. In addition, the graphene-carbon dot was stable to attach to the working electrode which was confirmed by CV for 40 cycles test (Fig. 3B). It showed a stable signal from the 1st to 40th cycles. Thus, the graphene-carbon dot material was suitable for MIP-based Aβ-42 sensor fabrication.
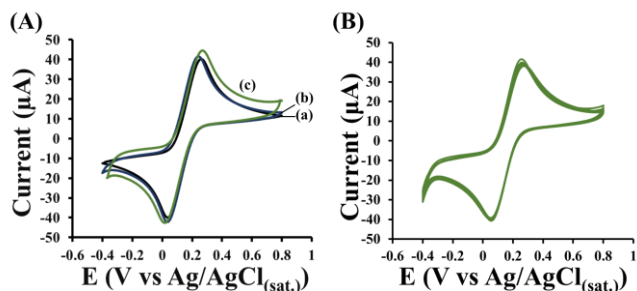

Fig. 3. The CV profiles (A) of bare SPCE (a), graphene (b) and graphene-carbon dot (c), (B) graphene-carbon dot /SPCE 40 cycles in 1 mM $K_3[Fe(CN)_6]/K_4[Fe(CN)_6]$ containing 0.1 M KCl.

C. MIP-Based Aβ-42 Electrochemical Characterizationf

DPV were also used to show the difference between MIP and NIP electrode. After polymerization (curve a of Fig. 4 A–B), NIP showed a higher current signal than MIP because it contained only oPD which is a conductive polymer. After elution (curve b of Fig. 4 A–B), the current signal of MIP was increased higher than NIP because Aβ-42 template was eluted out of the MIP pocket. After rebinding of Aβ-42 protein (curve c of Fig 4 A–B), the current signal of MIP was significantly decreased. The reduction of the current after rebinding of Aβ-42 could be explained by the presence of Aβ-42 protein as it consists of approximately 50% of nonpolar amino acids i.e. glycine, alanine, valine, leucine, isoleucine, and phenylalanine shown in (Fig. 2). These amino acids can interrupt the transfer of electron between the MIP pocket and $K_3[Fe(CN)_6]/K_4[Fe(CN)_6]$ solution. Meanwhile, NIP showed the same current signals for all steps as it allowed the same amount of electron transfer in all steps. These results suggests that we obtained distinguishable current signals between the MIP and NIP after rebinding with Aβ-42 (Fig. 4 C). Thus, the oPD polymer was suitable for the MIP-based Aβ-42 sensor production.
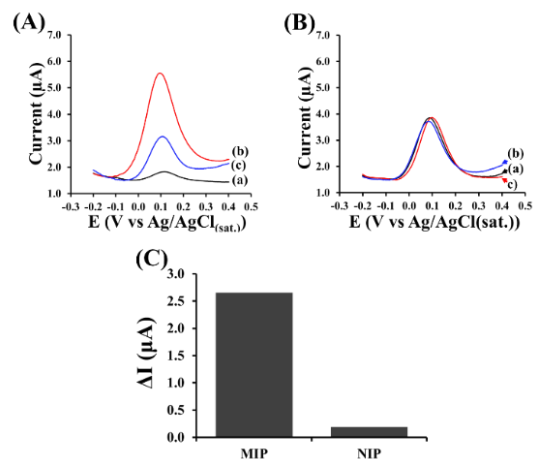

Fig. 4. The DPV profile of MIP (A) and NIP (B); after polymerization (a), after elution (b), and after Aβ-42 rebinding (c). The ΔI of MIP and NIP (C) in 1 mM K3[Fe(CN)6]/ K4[Fe(CN)6] containing 0.1 M KCl.

D. The Performance of MIP-Based Aβ-42 Sensor

The performances of MIP-based Aβ-42 sensor based on the number of CV cycle for electropolymerization and elution time were investigated by DPV technique. The thickness of MIP film is depended on the number of CV cycle of electropolymerization. Thus, the MIP-based Aβ-42 sensor was fabricated by varying the cycle number from 10 to 30 cycles. In Fig. 5(a), the results showed that the CV cycle of 15 cycles provided the maximum value of ΔI. On the other hand, the values of ΔI were decreased when the MIP was produced using electropolymerization cycle more than 15 cycles (20 and 30 cycles). This suggests that increasing the thickness of the MIP film might limit the accessibility of Aβ-42 protein in the MIP pocket site and also block electron transfer at the electrode surface resulting in decrease of the current response [15]. Thus, the number of CV of 15 cycles was properly used for MIP-based Aβ-42 sensor fabrication.

The second factor of MIP sensor is the elution time after MIP polymerization, the MIP/graphene-carbon dot/SPCE was immersed in the basic solution of NaOH (5mM) from 3 to 10 mins to elute out Aβ-42 protein template from the MIP pocket. Because of the strong basic condition, it directly affected the deprotonation of amino acids to deconstruct the Aβ-42 conformation resulting in the conformation change and the elution of the template from the recognition sites. To evaluate the performance of the elution time, the MIP modified electrode was incubated with Aβ-42 for 5 minutes to rebinding. As the result shown in Fig. 5(b), the ΔI values were increased from 3 to 8 minutes and then dramatically decreased to the lowest point at 10 minutes of elution. It is possible that the longer time of elution might deconstruct the oPD polymer of MIP, therefore; the MIP conformation was destroyed and it cannot form specific pocket sites to interact with Aβ-42. Thus, the optimum elution time was selected at 8 minutes.

Finally, the Aβ-42 sensor performance was validated using varied concentration of Aβ-42 of 0.5, 1, 5, 10, 20, and 30 pg/ml. The calibration curve showed a linear range of Aβ-42 from 0.5 to 20 pg/ml with the R^2 from the regression curve of 0.9732 and a limit of detection (LOD) of 0.104 ng/ml.
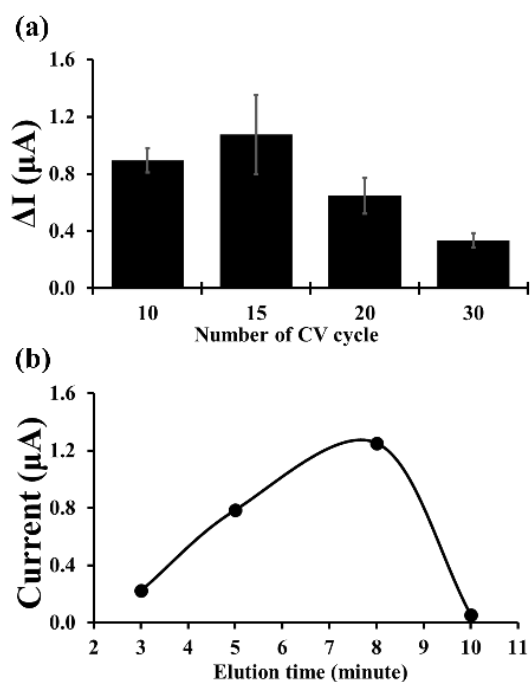
(a)

(b)

Fig. 5. The optimization of the number of CV cycle for electropolymerization (a) and elution time (b) by DPV in 1 mM $K_3[Fe(CN)_6]$/ $K_4[Fe(CN)_6]$ containing 0.1 M KCl.

$y = 0.079x + 1.8303$
$R^2 = 0.9732$
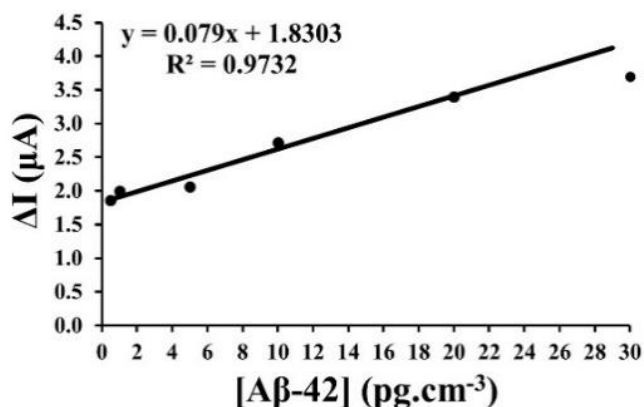
Fig. 6. The calibration curve of MIP-based Aβ-42 sensor.

IV. CONCLUSIONS

The graphene-carbon dot was successfully modified on SPCE. It can improve the electron transfer of the electrode. The oPD polymer was used as a polymer to fabricate the MIP-based Aβ-42 sensor. This sensor provided a linear range of Aβ-42 in the range of 0.5 to 20 pg/ml, with a LOD of 0.104 ng/ml. This is a simple fabrication of a MIP-based sensor that possess biomimetic sensor with good sensitivity, short response time, and low cost.

CONFLICT OF INTEREST

The authors declare no conflict of interest.

AUTHOR CONTRIBUTIONS

Conceptualization, R.P.P., N.P., and P.N.; methodology, R.P.P. and S.P.; validation, S.N., N.P. and P.N.; investigation, S.P. and S.N..; writing—original draft preparation, S.P. and S.N.; writing—review and editing, R.P.P. and N.P.;

visualization, S.N. All authors have read and agreed to the published version of the manuscript.

REFERENCES

[1] T. K. Khan, "Introduction to Alzheimer's disease biomarkers," in *Biomarkers in Alzheimer's Disease*, T. K. Khan, Ed. Academic Press, 2016, ch. 1, pp. 3–23.
[2] T. Qiu, Q. Liu, Y.-X. Chen, Y.-F. Zhao, and Y.-M. Li, "Aβ42 and Aβ40: Similarities and differences," *J. Pept. Sci.*, vol. 21, no. 7, pp. 522–529, 2015.
[3] G. Chen *et al.*, "Amyloid beta: Structure, biology and structure-based therapeutic development," *Acta Pharmacol. Sin.*, vol. 38, no. 9, Sep. 2017.
[4] "2020 Alzheimer's disease facts and figures," *Alzheimers Dement.*, vol. 16, no. 3, pp. 391–460, 2020. https://doi.org/10.1002/alz.12068
[5] T. K. Khan, "Alzheimer's disease Cerebrospinal Fluid (CSF) biomarkers," in *Biomarkers in Alzheimer's Disease*, T. K. Khan, Ed. Academic Press, 2016, ch. 5, pp. 139–180.
[6] T. K. Khan, "Peripheral fluid-based biomarkers of Alzheimer's disease," in *Biomarkers in Alzheimer's Disease*, T. K. Khan, Ed. Academic Press, 2016, ch. 6, pp. 183–218.
[7] I.-H. Cho, D. H. Kim, and S. Park, "Electrochemical biosensors: Perspective on functional nanomaterials for on-site analysis," *Biomater. Res.*, vol. 24, p. 6, Feb. 2020.
[8] F. R. Simões and M. G. Xavier, "Electrochemical sensors," in *Nanoscience and its Applications*, A. L. Da Róz, M. Ferreira, F. de Lima Leite, and O. N. Oliveira, Eds. William Andrew Publishing, 2017, ch. 6, pp. 155–178
[9] Y. Saylan, S. Akgönüllü, H. Yavuz, S. Ünal, and A. Denizli, "Molecularly imprinted polymer based sensors for medical applications," *Sensors*, vol. 19, no. 6, Jan. 2019.
[10] M. You, S. Yang, Y. An, F. Zhang, and P. He, "A novel electrochemical biosensor with molecularly imprinted polymers and aptamer-based sandwich assay for determining amyloid-β oligomer," *J. Electroanal. Chem.*, vol. 862, 114017, Apr. 2020.
[11] H. J. Yoo, B. E. Kwak, and D. H. Kim, "Interparticle distance as a key factor for controlling the dual-emission properties of carbon dots," *Phys. Chem. Chem. Phys.*, vol. 22, no. 36, pp. 20227–20237, Sep. 2020.
[12] S. K. Singh, S. Srivastav, A. K. Yadav, S. Srikrishna, and G. Perry, "Overview of Alzheimer's disease and Some therapeutic approaches targeting Aβ by using several synthetic and herbal compounds," *Oxid. Med. Cell. Longev.*, vol. 2016, 7361613, 2016.
[13] J. Phiri, P. Gane, and T. C. Maloney, "General overview of graphene: Production, properties and application in polymer composites," *Mater. Sci. Eng. B*, vol. 215, pp. 9–28, Jan. 2017.
[14] J. Liu, R. Li, and B. Yang, "Carbon dots: A new type of carbon-based nanomaterial with wide applications," *ACS Cent. Sci.*, vol. 6, no. 12, pp. 2179–2195, Dec. 2020.
[15] B. V. M. Silva, B. A. G. Rodríguez, G. F. Sales, M. D. P. T. Sotomayor, and R. F. Dutra, "An ultrasensitive human cardiac troponin T graphene screen-printed electrode based on electropolymerized-molecularly imprinted conducting polymer," *Biosens. Bioelectron.*, vol. 77, pp. 978–985, Mar. 2016.